Population accumulation in dark states and subrecoil laser cooling

M. R. Doery, M. T. Widmer, M. J. Bellanca, W. F. Buell, T. H. Bergeman, and H. Metcalf
Physics Department, State University of New York at Stony Brook, Stony Brook, New York 11794-3800

E. J. D. Vredenbregt
Physics Department, Eindhoven University of Technology, P.O. Box 513, 5600 MB Eindhoven, The Netherlands
(Received 21 February 1995)

The Λ system resulting from the interaction of counterpropagating orthogonally polarized beams of light with a $J_g = 1 \rightarrow J_e = 1$ transition is known to exhibit laser cooling without the presence of a damping force, through velocity selective coherent population trapping. This occurs independent of the sign of the laser's detuning from the atomic resonance frequency. We present measurements and calculations that show a detuning-dependent transient peak or dip in the ground-state momentum distribution centered at $p_g = 0$, however, which is reminiscent of laser cooling by a damping force. We explain this in terms of the character of the quantum-mechanical eigenstates of the total ground-state Hamiltonian of the system, using both analytic expressions and numerical calculations.

PACS number(s): 32.80.Pj, 42.50.Vk

In laser cooling of atoms, velocity selective coherent population trapping (VSCPT) occurs for particular configurations where the atom-laser system produces noncoupled states $|\mathrm{NC}\rangle$ that do not interact with the light [1,2]. This kind of laser cooling is distinguished from other types (e.g., Doppler [3] and polarization gradient cooling [4]) because it is not described by a damping force. Rather, atoms interacting with the laser light may decay into the noncoupled states via a random walk and then remain there. The atom-laser interaction is ineffective for these states, but the atomic kinetic energy causes a motional mixing between the $|\mathrm{NC}\rangle$ states and other states $|\mathrm{C}\rangle$ that *are* coupled. VSCPT occurs when this motional coupling depends on momentum p in such a way that it vanishes for a certain noncoupled state, the *trapped state* $|\mathrm{NC}(p = 0)\rangle$ [1,2]. In the first discussions of VSCPT, it was shown that for counterpropagating orthogonally polarized beams of light, in either the σ^+-σ^- (orthogonal circular polarizations) or lin⊥lin (orthogonal linear polarizations) configurations on a $J_g = 1 \rightarrow J_e = 1$ transition, there is a Λ system (Fig. 1) that contains such a trapped state.

Although it is possible for cooling forces to operate in the presence of VSCPT in some cases [5–8], it has been shown that no such force is present for the commonly studied arrangements of one-dimensional σ^+-σ^- and lin⊥lin polarizations applied to a $J_g = 1 \rightarrow J_e = 1$ transition, as found in metastable helium for $2\,^3S_1 \rightarrow 2\,^3P_1$ [2,5,9]. Thus it is not expected that the sign of δ, where $\delta = \omega_l - \omega_a$ is the laser detuning from the atomic resonance frequency, will affect the cooling process, as it does in laser cooling caused by a damping force. Indeed, it has been found both theoretically and experimentally that VSCPT is efficient independently of the sign of the detuning [2,5,9,10]. Nevertheless, in [2] a difference in the finite-time ground-state momentum distribution $\mathcal{P}(p_g, t)$ about $p_g = 0$ was found to be associated with the sign of δ. The momentum distribution between the characteristic narrow VSCPT cold peaks in $\mathcal{P}(p_g, t)$ at $p_g = \pm\hbar k$ was elevated for positive detuning and depressed for negative detuning (see Fig. 10 and Sec. 6.E of [2], as well as Fig. 6 herein). Kaiser [11] has discussed this phenomenon in terms of the coherence (off-diagonal atomic density-matrix element) between the $|\mathrm{NC}\rangle$ and $|\mathrm{C}\rangle$ states.

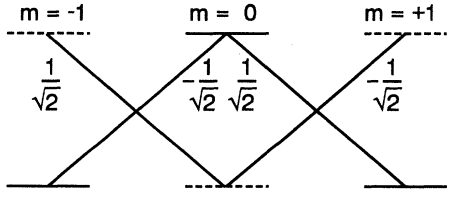

FIG. 1. Circularly polarized light applied to the $J_g = 1 \rightarrow J_e = 1$ system. The $m_g = 0 \leftrightarrow m_e = 0$ transition is forbidden, so that atoms eventually depopulate the V system and only occupy the Λ system.

In recent experiments and numerical calculations using the lin⊥lin polarization configuration with metastable helium atoms [10], we have observed that for nonzero detuning, there are many cases where there is a central structure at $p_g = 0$, but the typical VSCPT peaks at $p_g = \pm\hbar k$ are *not* evident. Specifically, for positive detuning we find an overpopulation of slow atoms resulting in a single narrow peak in $\mathcal{P}(p_g, t)$ centered at $p_g = 0$, and for negative detuning a dip (see Fig. 2). This structure generally has a full width at half maximum of only approximately $2\hbar k$, indicating that it is not the result of currently known laser-cooling mechanisms. With positive detuning, this presents an alternative method for producing a single cold peak of atoms. Furthermore, the detuning dependence of the momentum distribution can be used in conjunction with conventional saturation spectroscopy as a measure of laser detuning (see discussion below). Finally, we have found that the origin of this very narrow structure in $\mathcal{P}(p_g \approx 0, t)$ is analytically tractable, which provides insight into this laser-cooling configuration.

In this paper, we treat the problem in the basis of the

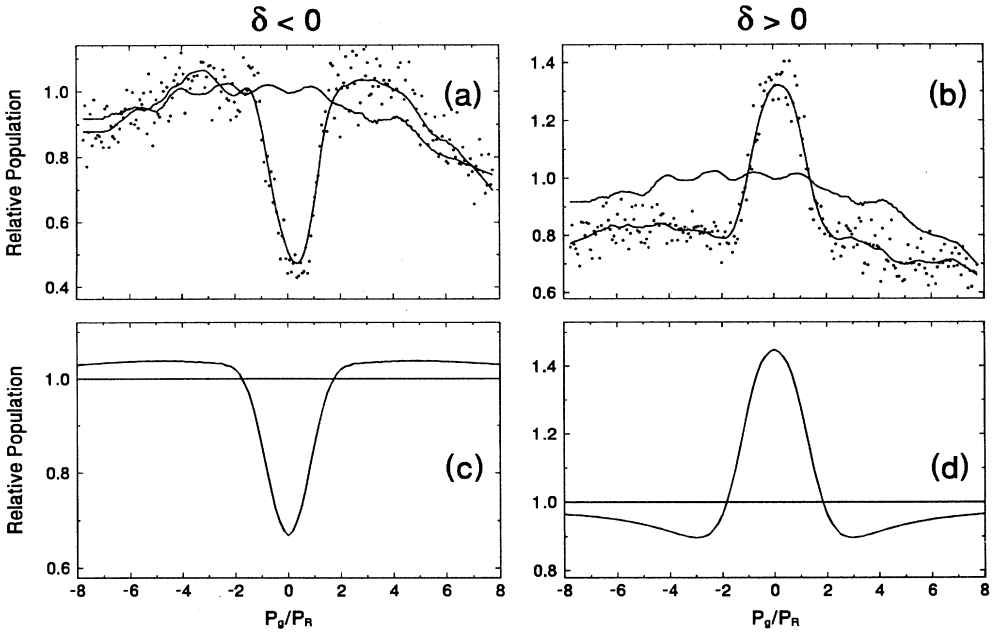

FIG. 2. Measured and calculated momentum distributions for the lin⊥lin case on the $2\,^3S_1 \rightarrow 2\,^3P_1$ transition of metastable He atoms. $\mathcal{P}(p_g,t)$ is highly dependent on the sign of the detuning. Here $S = 12$ and (a) $\delta \approx -8\Gamma$ and (b) $\delta \approx 8\Gamma$. The total interaction time $T_{\max} = 200\Gamma^{-1}$. The experimental distributions are normalized so that the initial distribution has height approximately equal to 1. Actual scatter of data points at $T_{\max}$ is plotted, along with a smoothed curve through the initial and final momentum distributions. The results of numerical calculations are shown in (c) and (d), for corresponding laser parameters.

eigenstates of the complete ground-state Hamiltonian of the system, including the kinetic-energy operator for the atomic center-of-mass motion, rather than the coupled and noncoupled eigenstates $|\mathrm{C}\rangle$ and $|\mathrm{NC}\rangle$ of the ground-state atom-field interaction term alone. Thus we depart from the more common approach for VSCPT. We examine the configuration of counterpropagating orthogonally polarized beams of light in one dimension on a Λ system; we discuss in detail the case of σ^+-σ^- polarizations and show that similar arguments may be developed and similar conclusions reached for the lin⊥lin case. Our calculations are supported by quantitative agreement with measurements. A brief discussion of our numerical calculations and experimental setup is provided after the analytical discussion.

The time evolution of the atomic density matrix is determined by the generalized optical Bloch equations

$$i\hbar\dot{\rho} = [H_{\mathrm{tot}}, \rho] + i\hbar\Gamma\rho_{\mathrm{repop}}, \tag{1}$$

with Γ the excited-state spontaneous decay rate and ρ_{repop} a shorthand notation for terms that account for decay [12]. The total Hamiltonian for our system is

$$H_{\mathrm{tot}} = \frac{P^2}{2M} + \hbar\omega_a \sum_e |e\rangle\langle e| + H_{al}, \tag{2}$$

where the sum is over the excited states involved. In the electric-dipole approximation, the atom-laser interaction H_{al} is given by the product of the laser's electric field with the dipole moment operator $H_{al} = -\mathbf{E}\cdot\mathbf{D}$. For counterpropagating σ^+-σ^- waves the laser's electric field is

$$\begin{aligned}\mathbf{E} &= E_0\hat{\mathbf{x}}\{\cos(kz-\omega t)+\cos(kz+\omega t)\} \\ &\quad -E_0\hat{\mathbf{y}}\{\sin(kz-\omega t)+\sin(kz+\omega t)\} \\ &= \frac{E_0}{\sqrt{2}}\{\hat{\boldsymbol{\epsilon}}_+ e^{ikz} + \hat{\boldsymbol{\epsilon}}_- e^{-ikz}\}e^{-i\omega t} + \text{c.c.},\end{aligned} \tag{3}$$

with $\hat{\boldsymbol{\epsilon}}_+ = \frac{\hat{\mathbf{x}}+i\hat{\mathbf{y}}}{\sqrt{2}}$ and $\hat{\boldsymbol{\epsilon}}_- = \frac{\hat{\mathbf{x}}-i\hat{\mathbf{y}}}{\sqrt{2}}$. Hence the interaction is

$$\begin{aligned}H_{al} &= \frac{\hbar\Omega}{2\sqrt{2}}\left\{e^{-ikZ}|0_e\rangle\langle 1_g| - e^{ikZ}|0_e\rangle\langle -1_g|\right\} \\ &\quad \times e^{-i\omega t} + \text{H.c.} \qquad (4) \\ &\equiv W_{eg}e^{-i\omega t} + W_{ge}e^{i\omega t}, \qquad (5)\end{aligned}$$

where we have used the rotating-wave approximation and restrict the analysis to the Λ system that connects the states $|-1_g\rangle$, $|0_e\rangle$, and $|1_g\rangle$ (see Fig. 1). The single-beam Rabi frequency Ω is related to the experimental saturation parameter by $S = 2\Omega^2/\Gamma^2$, the laser intensity $I = Shc\Gamma k^3/24\pi^2$ and for circularly polarized light $\hbar\Omega = -E_0 d_0\sqrt{2}$, where $d_0 = (3\pi\epsilon_0\hbar\Gamma/k^3)^{\frac{1}{2}}$ is the reduced matrix element of the dipole moment. Atomic motion is treated quantum mechanically in the expression for H_{al}, so z becomes the atomic position operator Z.

In the low excitation regime, where the detuning and the saturation parameter satisfy $S/L \ll 1$, with $L = 1 + 4\delta^2/\Gamma^2$, we can adiabatically eliminate the excited states to obtain the equations of motion for ground-state elements alone, $\tilde{\rho} = \rho_{gg'}$ [4,13–15]:

$$\begin{aligned}i\hbar\dot{\tilde{\rho}} &= \frac{1}{2M}[P^2,\tilde{\rho}] + \frac{4\delta}{\hbar\Gamma^2 L}[A,\tilde{\rho}] - \frac{2i}{\hbar\Gamma L}\{A,\tilde{\rho}\}_+ \\ &\quad + \frac{i\hbar\Gamma}{L}\sum_{\sigma=-1}^{1}\int_{-\hbar k}^{\hbar k} dp'\mathcal{N}_\sigma(p')[R_\sigma(p')]^\dagger\tilde{\rho}R_\sigma(p').\end{aligned} \tag{6}$$

The operator $A = \sum_e W_{ge}W_{eg'}$. The third term, an anticommutator, accounts for optical pumping out of the ground states, while the last term repopulates them. $R_\sigma(p')$ accounts for decay from the excited state, including momentum recoil and Clebsch-Gordan coefficients, and $\mathcal{N}_\sigma(p')$ is the radiation pattern associated with the linearly or circularly polarized light, denoted by the sub-

script σ, emitted during spontaneous emission [4].

In analogy to Eq. (1), these ground-state equations of motion have a Hamiltonian-like part H_{eff}, which is the sum of a kinetic-energy term and an effective potential $V_{\text{eff}} = 4\delta A/\hbar\Gamma^2 L$. V_{eff} is block diagonal in the momentum basis; here we write a representative block for one particular "family momentum" p [2],

$$\begin{aligned} V_{\text{eff}}(p) = \frac{U_0}{2}\{&|p+1,1_g\rangle\langle p+1,1_g| \\ &-|p+1,1_g\rangle\langle p-1,-1_g| \\ &-|p-1,-1_g\rangle\langle p+1,1_g| \\ &+|p-1,-1_g\rangle\langle p-1,-1_g|\}, \end{aligned} \tag{7}$$

where we have defined $U_0 \equiv S\hbar\delta/2L$ and we have adopted the convention of expressing the momentum p in units of the recoil momentum $\hbar k$, effectively making p into a unitless number. Our state kets are products of internal states with momentum operator eigenstates $|p,m\rangle = |p\rangle|m\rangle$ and we have used the relation $e^{\pm ikZ} = \int_{-\infty}^{\infty} dp|p\rangle\langle p \mp 1|$ [2].

Traditionally VSCPT has been treated using the eigenbasis of *only* the effective potential V_{eff}, sometimes called the "optical basis." Diagonalizing V_{eff} yields a set of orthonormal states $|\text{NC}\rangle$ and $|\text{C}\rangle$ for any particular family momentum p,

$$|\text{NC}(p)\rangle = \frac{1}{\sqrt{2}}\{|p+1,1_g\rangle + |p-1,-1_g\rangle\}, \tag{8}$$

$$|\text{C}(p)\rangle = \frac{1}{\sqrt{2}}\{|p+1,1_g\rangle - |p-1,-1_g\rangle\}, \tag{9}$$

as discussed in [2]. The noncoupled state does not interact with the laser light, $V_{\text{eff}}|\text{NC}(p)\rangle = 0$. On the other hand, $|\text{C}\rangle$ does interact strongly with the light, $V_{\text{eff}}|\text{C}(p)\rangle = U_0|\text{C}(p)\rangle$. Due to the kinetic-energy part of the Hamiltonian, an atom in the noncoupled state will evolve out of it into the coupled state in most cases. It is only trapped in the $|\text{NC}\rangle$ state at family momentum $p = 0$, where this "motional mixing" (which is proportional to p) is zero.

Our approach is different from this traditional one because we work with the eigenbasis of the *entire* effective Hamiltonian of the Λ system $H_{\text{eff}} = P^2/2M + V_{\text{eff}}$. Working with these eigenstates of the system gives an added insight, which, in conjunction with the more usual approach, leads to an intuitive explanation for the detuning-dependent effect described in the opening paragraphs.

H_{eff} is block diagonal in the family momentum p, so we determine the eigenstates by solving the Schrödinger equation for a representative p, $H_{\text{eff}}(p)\Psi(p) = E(p)\Psi(p)$. Writing this explicitly using the recoil energy $E_R = \hbar^2k^2/2M$ we get

$$\left[P^2 - \frac{E}{E_R} + \frac{1}{E_R}V_{\text{eff}}(p)\right]|\Psi(p)\rangle = 0. \tag{10}$$

Choosing a solution of the form

$$|\Psi(p)\rangle = \xi(p)|p-1,-1_g\rangle + \zeta(p)|p+1,1_g\rangle \tag{11}$$

and substituting $u = U_0/2E_R$ we obtain the eigenvalues

$$\left(\frac{E}{E_R}\right)_{\pm} = u + p^2 + 1 \pm \sqrt{u^2+4p^2} \tag{12}$$

and the coefficients for the associated eigenvectors

$$\begin{aligned} \xi_{\pm}(p) &= -\frac{u}{N_{\pm}}, \\ \zeta_{\pm}(p) &= \frac{1}{N_{\pm}}\left\{2p \pm \sqrt{u^2+4p^2}\right\}, \end{aligned} \tag{13}$$

where

$$N_{\pm} = \sqrt{u^2 + \left(2p \pm \sqrt{u^2+4p^2}\right)^2}. \tag{14}$$

These eigenfunctions of the effective Hamiltonian may be expanded in the optical basis $|\Psi_{\pm}\rangle = \alpha_{\pm}|\text{NC}\rangle + \beta_{\pm}|\text{C}\rangle$ where $\alpha_{\pm}^*\alpha_{\pm} + \beta_{\pm}^*\beta_{\pm} = 1$. The quantity $\alpha_{\pm}^*\alpha_{\pm}$ is a measure of how well the eigenstates of H_{eff} may be approximated as eigenstates of V_{eff}, as a function of p:

$$|\alpha_{\pm}|^2 = \frac{1}{2N_{\pm}^2}\left\{-u + 2p \pm \sqrt{u^2+4p^2}\right\}^2. \tag{15}$$

A plot of $|\alpha_{\pm}|^2$ vs p is given in Fig. 3 for two different values of U_0. We see that for $p^2 \ll (U_0/E_R)^2$, $|\alpha_{\pm}|^2$ is nearly unity, meaning that the eigenfunctions are closely related to the states of the optical basis. This is because the effective potential dominates over the kinetic-energy term in H_{eff} when p is small. In particular, $|\Psi_{\pm}(p=0)\rangle$ are exactly the $|\text{NC}\rangle$ and $|\text{C}\rangle$ states. For $\delta > 0$, $|\Psi_-(p=0)\rangle = |\text{NC}(p=0)\rangle$ and $|\Psi_+(p=0)\rangle = |\text{C}(p=0)\rangle$ and vice versa for $\delta < 0$. Hence we call the eigenstates of H_{eff} "weakly coupled" and "strongly coupled," $|\text{WC}\rangle$ and $|\text{SC}\rangle$.

Spontaneous emission causes atomic population to build up in the weakly coupled manifold, with a corresponding drop in the population of the strongly coupled manifold. The two manifolds are clearly distinguishable

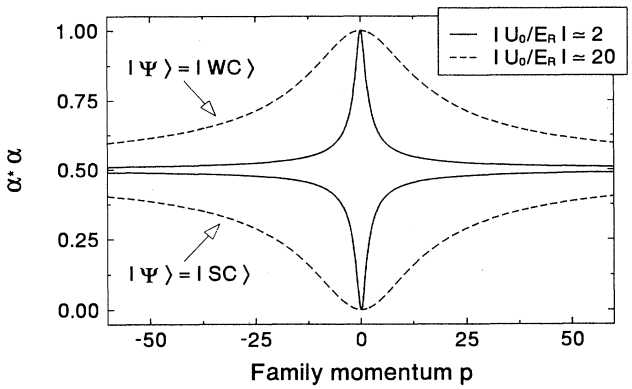

FIG. 3. Eigenstates of H_{eff} may be written $|\Psi_{\pm}\rangle = \alpha_{\pm}|\text{NC}\rangle + \beta_{\pm}|\text{C}\rangle$. The figure shows $|\alpha_{\pm}|^2$ as a function of p, for the σ^+-σ^- case, for two different values of $U_0 = S\hbar\delta/2L$: (a) $|U_0/E_R| \approx 2$ and (b) $|U_0/E_R| \approx 20$. This function is a calculation of the projection of the eigenstates of H_{eff}, namely, $|\text{WC}\rangle$ and $|\text{SC}\rangle$ onto the eigenstates of the effective potential V_{eff}, namely, $|\text{NC}\rangle$ and $|\text{C}\rangle$.

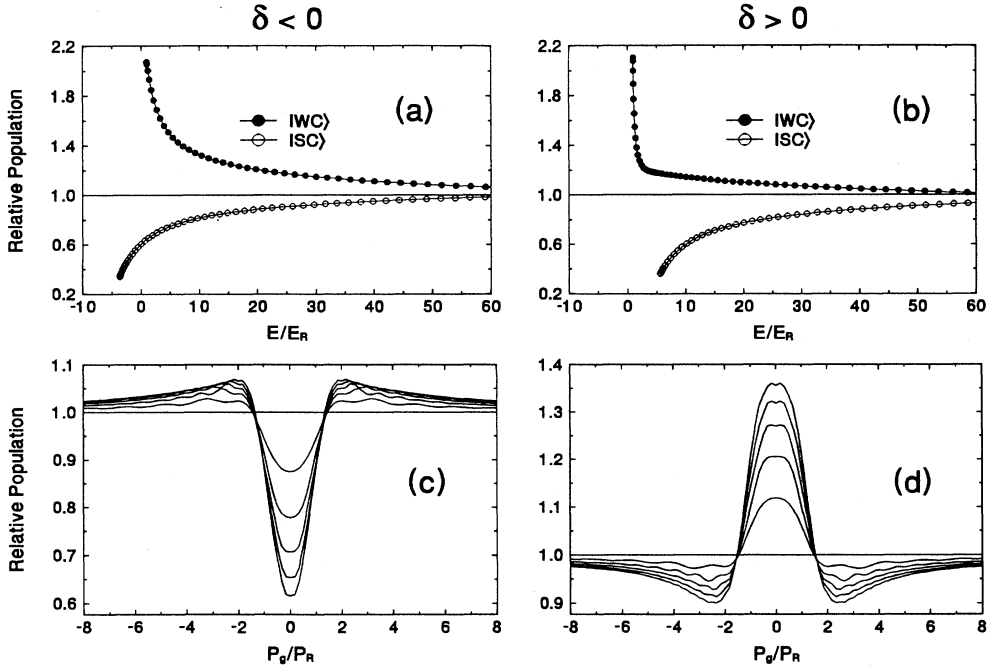

FIG. 4. Plot of the atomic population at total interaction time $T_{\max} = 200\Gamma^{-1}$, as a function of the energy eigenvalues of H_{eff}, for (a) $\delta = -8\Gamma$ and (b) $\delta = 8\Gamma$. In both cases the weakly coupled manifold of eigenstates has become overpopulated at the expense of the strongly coupled manifold. The time evolution of the corresponding momentum distributions are quite distinct; for (c) $\delta < 0$, a dip becomes deeper, but for (d) $\delta > 0$, a peak grows (successive time increments of $T_{\text{inc}} = 40\Gamma^{-1}$ are shown). These calculations were performed for the He transition of Fig. 2, but for the σ^+-σ^- case and with $S = 8$.

in Fig. 4, where the calculated atomic He* population is plotted as a function of energy eigenvalue for an interaction time of $200\Gamma^{-1}$, detuning $\delta = \pm 8\Gamma$, and saturation parameter $S = 8$. The initial momentum distribution $\mathcal{P}(p_g, t = 0)$ is uniform with unit height from $p_g = -15\hbar k$ to $p_g = +15\hbar k$. The corresponding energy distribution is obtained by projecting onto the basis of eigenstates of H_{tot} and is also normalized to unit height. The population is plotted relative to this initial distribution.

Regardless of the sign of the detuning, the weakly coupled manifold is always overpopulated. There is very little difference in the atomic energy distributions when the sign of the detuning is changed. However, the effect of changing the sign of δ is quite apparent for the corresponding atomic momentum distributions also shown in Fig. 4. There is a narrow peak centered at $p_g = 0$ for $\delta > 0$, but a dip instead for $\delta < 0$.

This phenomenon is caused by the way in which the eigenfunctions of H_{eff} are composed of particular ground-state momenta p_g. In particular, we find that one manifold of eigenstates has no contribution from $|p_g| < 1$, whereas the other manifold is composed of all ground-state momenta, including $|p_g| < 1$. We can develop some intuition for this by looking at the eigenvalues when u is very small. In that case, the kinetic-energy term begins to dominate H_{eff} at $|p| \gtrsim 1$. From Eq. (12), the dispersion relations for $|u| \ll 1$ are approximately

$$\left(\frac{E}{E_R}\right)_{\pm} \approx u + (p \pm 1)^2. \tag{16}$$

These two parabolas (shifted by the constant u) give the energies of the "free-particle" states $|p \pm 1\rangle$, which are composed of ground-state momenta $p_g = (p \pm 1)\hbar k$ [16]. In Fig. 5 we plot the energies of these free-particle states, as well as the exact formulas from Eq. (12), as a function of p. There is a small anticrossing of the parabolas at $p = 0$, where $p_g = \pm\hbar k$. For $\delta > 0$, the weakly coupled manifold is the curve below the anticrossing. Notice that this curve contains all ground-state momenta, in particular $|p_g| < 1$. On the other hand, the strongly coupled manifold, above the anticrossing, has *no* contribution from $|p_g| < 1$ (apart from the small amount of mixing due to the anticrossing). In Fig. 5 we have labeled the energy curves to indicate what ground-state momenta they are composed of, and relative population is indicated by filled (empty) circles for the $|\text{WC}\rangle$ ($|\text{SC}\rangle$) states. Since atoms accumulate in the $|\text{WC}\rangle$ states, this means that ground-state momenta $|p_g| < 1$ are overpopulated and a peak occurs around $p_g = 0$ in the momentum distribution. When $\delta < 0$, the reverse is true: the weakly coupled manifold is above the anticrossing and does not contain $|p_g| < 1$ states; instead, the depleted strongly coupled manifold contains $|p_g| < 1$ and so we see a dip in the momentum distribution.

Even when the $|\text{NC}(p = 0)\rangle$ state is most populated as in Fig. 4, VSCPT peaks at $\pm\hbar k$ may not be evident. In that case, the overpopulation of the VSCPT trapped state $|\text{WC}(p = 0)\rangle = |\text{NC}(p = 0)\rangle$ which is composed of $p_g = \pm\hbar k$, is accompanied by an approximately equal *underpopulation* of $|\text{SC}(p = 0)\rangle = |\text{C}(p = 0)\rangle$, which is *also* composed of $p_g = \pm\hbar k$. However, for long enough interaction times, the trapped state becomes so overpopulated relative to all other states that it is the dominant structure in $\mathcal{P}(p_g, t)$. It is only then that the narrow peaks at $\pm\hbar k$ become distinguishable (see Fig. 6).

We have found that using saturation parameters S not much larger than 1 and $\delta \approx 0$ is favorable for the

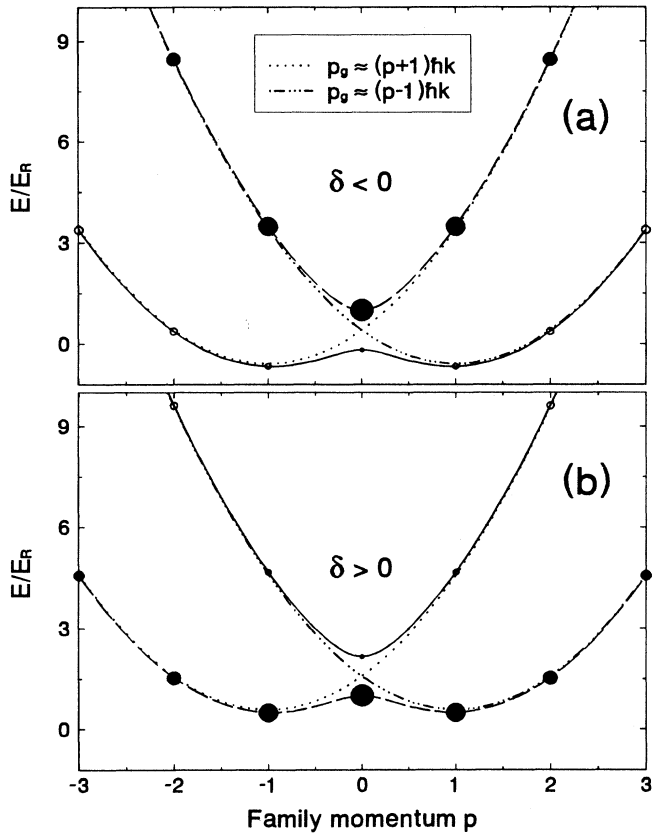

FIG. 5. Dispersion relations for small $|U_0/E_R|$, as given by Eqs. (12) and (16). When $U_0/E_R \neq 0$, there is an anticrossing at $p = 0$, as well as a vertical shift. The weakly coupled state $|\mathrm{WC}(p=0)\rangle = |\mathrm{NC}(p=0)\rangle$ has a fixed energy eigenvalue of $E/E_R = 1$, independent of U_0/E_R. (a) For $\delta < 0$, the upper curve is the weakly coupled manifold and the lower curve contains the strongly coupled eigenstates. Circles schematically represent where population accumulates. (b) Same as in (a), only now $\delta > 0$. In this case, the strongly coupled manifold is light-shifted upward and the weakly coupled manifold is the lower curve.

production of the well-separated and narrow VSCPT peaks at $\pm\hbar k$, with our experimental interaction times of $T_{\max} = 200\Gamma^{-1}$. This is consistent with the results of Aspect *et al.* [2], who showed in addition that the width of VSCPT peaks varies linearly with Rabi frequency (recall $S = 2\Omega^2/\Gamma^2$).

On the other hand, a different region of parameter space must be visited to obtain the single detuning-dependent peak/dip at $p_g = 0$. This narrow central structure is most clearly apparent when both S and $|\delta|$ are relatively large. Typically, we have used $4 < S < 12$ and $4 < |\delta/\Gamma| < 10$ when $T_{\max} = 200\Gamma^{-1}$. Note that Figs. 6(c) and 6(d) indicate that even for parameters outside this range, the momentum distribution initially passes through a stage where the central structure dominates and only then passes on to the stage where VSCPT peaks dominate.

Figures 2, 4, and 6 present the momentum and energy distributions of the diagonal elements of the atomic density matrix (populations). The method we have used for calculating the temporal evolution of the density matrix has been detailed elsewhere for other laser-cooling configurations [15,17] and we only summarize it here. We use Eq. (2) in Eq. (1), which is then rewritten in Liouvillean form $i\hbar\dot{\rho} = T\rho$, where the density matrix is evaluated over a basis of free-particle states $|p,m\rangle$. This large system of differential equations is solved numerically and the momentum distribution is then determined by taking the trace over magnetic sublevels m of the atomic populations. Alternatively, the density matrix is transformed to the basis of eigenfunctions of the total Hamiltonian H_{tot} and then atomic populations are plotted against the eigenvalues of H_{tot} to produce an energy distribution. The energy distributions in Figs. 4 and 6 were produced in this way; however, the excited-state populations were not plotted there since they are several orders of magnitude smaller than the ground-state populations. We have also numerically solved Eq. (6), now writing a Liouville equation for the ground-state elements alone, $i\hbar\dot{\tilde{\rho}} = \tilde{T}\tilde{\rho}$. For this case we have also determined both momentum and energy distributions, now using the eigenstates of the ground-state Hamiltonian H_{eff} for the latter type of distribution. When $S/L \ll 1$ these ground-state calculations agree well with the calculations that include the excited state; all numerical results presented in Figs. 2, 4, and 6 were obtained with the latter method.

The lin⊥lin case is quite similar to, but slightly more complicated than, the σ^+-σ^- case [18]. Here we present the main results. The laser field is created by counterpropagating laser beams that are linearly polarized orthogonal to each other, so we take $\hbar\Omega = -E_0 d_0$. The electric field is now written

$$\mathbf{E} = \frac{E_0}{\sqrt{2}}\{\hat{\boldsymbol{\epsilon}}_+ \cos kz - \hat{\boldsymbol{\epsilon}}_- \sin kz\}e^{-i\omega t} + \mathrm{c.c.} \tag{17}$$

and

$$H_{al} = -\frac{\hbar\Omega}{2}\{|0_e\rangle\langle -1_g| \cos kz + |0_e\rangle\langle 1_g| \sin kz\} \times e^{-i\omega t} + \mathrm{H.c.} \tag{18}$$

Once again we find a V_{eff} that is block diagonal in p, and using this we obtain solutions to Eq. (10):

$$|\Psi(p)\rangle = \frac{1}{\sqrt{2}}\{\xi|p-1,-1_g\rangle + i\xi|p-1,1_g\rangle + \zeta|p+1,1_g\rangle + i\zeta|p+1,-1_g\rangle\}, \tag{19}$$

with ζ and ξ as given in Eq. (13). The associated eigenvalues are again given by Eq. (12). The noncoupled state is now

$$|\mathrm{NC}\rangle = \frac{1}{2}\{e^{-i\pi/4}|p-1,-1_g\rangle + e^{i\pi/4}|p+1,-1_g\rangle + e^{i\pi/4}|p-1,1_g\rangle + e^{-i\pi/4}|p+1,1_g\rangle\} \tag{20}$$

so that the projection of the eigenstates onto the noncoupled states is again given by $|\alpha_\pm|^2$ as defined in Eq. (15)

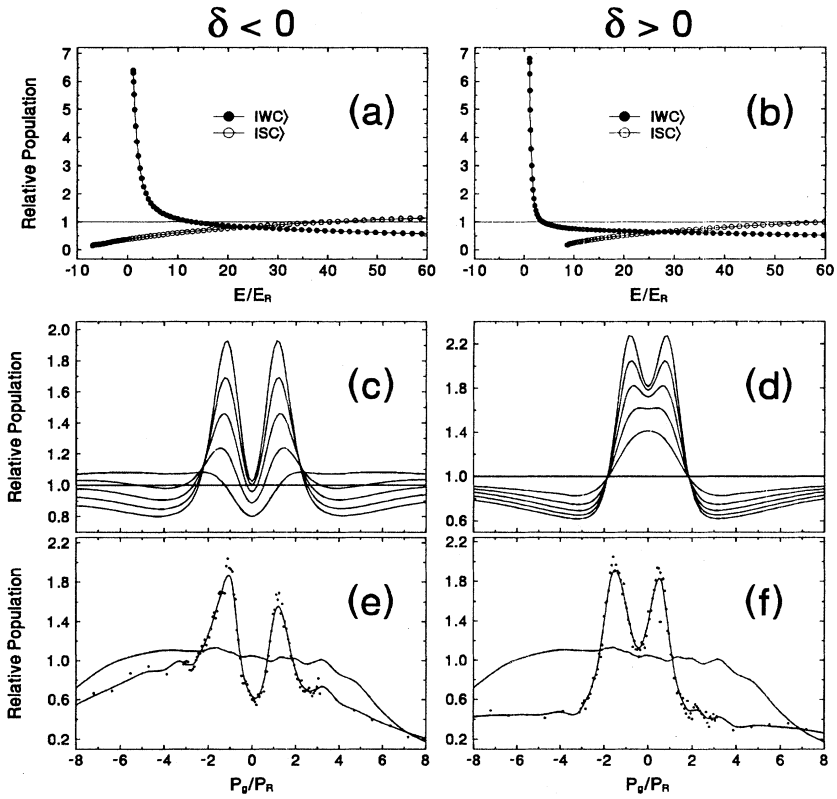

FIG. 6. lin⊥lin case, $S = 2, |\delta| = 1\Gamma$ on He^*. In (a) and (b) the calculated energy distributions at $T_{max} = 200\Gamma^{-1}$ are shown. The time evolution of the corresponding momentum distributions are plotted in (c) and (d), with time increments of $T_{inc} = 40\Gamma^{-1}$. For these parameters, by T_{max}, the trapped state is so highly populated that it dominates the momentum distribution, creating the typical VSCPT peaks at $p_g = \pm\hbar k$, though detuning dependence is still evident. In (e) and (f) the experimental results for similar laser parameters are plotted, showing an analogous structure.

and the same explanation of the detuning dependence that was given for the σ^+-σ^- case applies.

Figures 2 and 6 show measured and calculated momentum distributions in the case of the lin⊥lin polarization configuration. In Fig. 6 the usual VSCPT peaks at $\pm\hbar k$ are quite evident, but we still see that the region between the peaks at $p_g \approx 0$ is depressed or elevated depending on the sign of the detuning. A plot of the energy distribution is also given to demonstrate the existence of two manifolds of eigenstates $|WC\rangle$ and $|SC\rangle$.

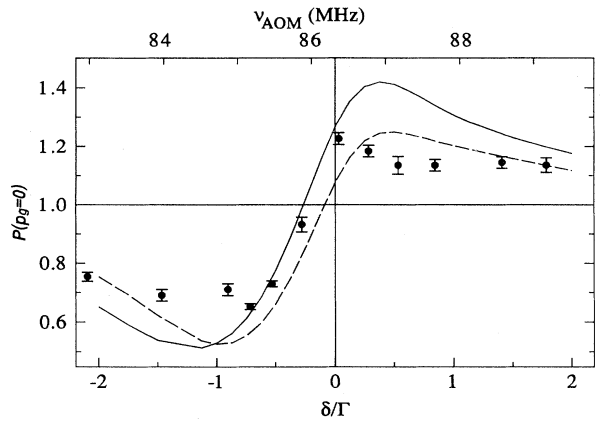

FIG. 7. Comparison of experimentally and numerically determined $\mathcal{P}(p_g = 0, T_{max}; \delta)$. The experimental interaction time is $T_{max} \simeq 100\Gamma^{-1}$ and the measured laser intensity maximum is $S_{max} = 0.94$. Numerical results are shown for $S_{max} = 1.0$ (solid line) and $S_{max} = 0.75$ (dashed line). The experimental curve has been shifted horizontally to be aligned as closely as possible to the numerically obtained curve. In this way the experimental parameter ν_{AOM}, as given in the top horizontal axis, may be related to laser detuning δ (bottom axis).

We have studied these effects experimentally for the lin⊥lin case using apparatus that has been described elsewhere [19], but is briefly presented here. Metastable $2\,^3S_1$ helium (He^*) atoms are produced by a dc-discharge-excited supersonic nozzle source cooled by liquid N_2. About 1 cm downstream of the nozzle is a conical skimmer followed 25 cm further downstream by a 30 μm × 7 mm collimation slit. Directly after this slit, the atoms interact with two counterpropagating laser beams with orthogonal linear polarizations that excite the $2\,^3S_1 \rightarrow 2\,^3P_1$ transition in He^* at 1.083 μm. The natural linewidth is $\Gamma/2\pi = 1.6$ MHz. The laser beams originate from a homebuilt laser diode end-pumped cw hexagonal lanthanum neodymium hexa-aluminate (Nd:LNA) laser [20,21] and have a nearly Gaussian profile with waist equal to 1.6 cm. The transverse velocity distribution of the He^* beam, modified by the interaction with the laser light, is measured 1.8 m downstream with a multichannel plate detector mounted behind a movable 35-μm slit. The longitudinal velocity distribution from the supersonic nozzle is 240 m/s wide and centered at 1600 m/s; the two slits separated by 1.8 m provide a velocity resolution of 4.4 cm/s or $\Delta p \simeq 0.5\hbar k$.

The laser frequency is tuned near the $2\,^3S_1 \rightarrow 2\,^3P_1$ transition using an offset locking scheme based on Zeeman tuned saturation spectroscopy [22] in a He rf discharge in a longitudinal magnetic field $B \approx 40$ G. The Zeeman shift ω_Z of the He^* atoms is compensated with

a frequency shift $\nu_{\mathrm{AOM}} \approx 85$ MHz from an acousto-optic modulator (AOM); this shifted beam is always locked to exact resonance with the Zeeman shifted transition, while the frequency of the unshifted main laser beam is lower by an amount ν_{AOM}. The laser detuning from resonance is then $\delta = \omega_Z - \nu_{\mathrm{AOM}}$. For a fixed interaction time $T_{\max}$ and laser saturation parameter S, the calculated $\mathcal{P}_0(\delta) \equiv \mathcal{P}(p_g = 0, T_{\max}; \delta)$ is plotted against detuning δ. This is matched to a similar experimental plot using the same $T_{\max}$ and S, only now the height of the momentum distribution at $p_g = 0$ is plotted vs ν_{AOM}. By aligning the experimentally obtained curve with that obtained numerically, a correspondence between ν_{AOM} and δ may be made. An example of this procedure is shown in Fig. 7. It is evident from the figure that the detuning dependence of $\mathcal{P}_0(\delta)$ is asymmetric and that the curve does not necessarily cross $\mathcal{P}_0 = 1$ at $\delta = 0$. The details of the shape of the curve are dependent on laser intensity and interaction time as well. Nevertheless, the steep slope in the region of $\delta = 0$ makes this feature useful in conjunction with conventional saturation spectroscopy for determination of the absolute laser detuning. The detunings derived using this procedure are found to be consistent with those from saturation spectroscopy.

In conclusion, we have presented numerical and experimental results showing that even for significant interaction times, a detuning-dependent peak or dip is sometimes the only observable feature in even the simplest VSCPT configuration. This peak may contain a significant fraction of the atoms and have a rms width less than $1\hbar k$. We have developed an intuitive analytical model based on the character of the eigenstates of the problem that accounts for this narrow structure. Thus VSCPT in the low excitation regime can profitably be discussed using the eigenstates of the effective ground-state Hamiltonian, which includes kinetic energy as well as the effective potential. This approach complements the traditional method, which uses the eigenbasis of the effective potential alone.

This work was supported by the NSF, the ONR, a NATO travel grant, and a grant of computer time from the Cornell Theory Center.

[1] A. Aspect, E. Arimondo, R. Kaiser, N. Vansteenkiste, and C. Cohen-Tannoudji, Phys. Rev. Lett. **61**, 826 (1988).
[2] A. Aspect, E. Arimondo, R. Kaiser, N. Vansteenkiste, and C. Cohen-Tannoudji, J. Opt. Soc. Am. B **6**, 2112 (1989).
[3] P. D. Lett, W. D. Phillips, S. L. Rolston, C. E. Tanner, R. N. Watts, and C. I. Westbrook, J. Opt. Soc. Am. B **6**, 2084 (1989).
[4] J. Dalibard and C. Cohen-Tannoudji, J. Opt. Soc. Am. B **6**, 2023 (1989).
[5] M. S. Shahriar, P. R. Hemmer, M. G. Prentiss, P. Marte, J. Mervis, D. P. Katz, N. P. Bigelow, and T. Cai, Phys. Rev. A **48**, R4035 (1993).
[6] M. Weidemüller, T. Esslinger, M. A. Ol'shanii, A. Hemmerich, and T. W. Hänsch, Europhys. Lett. **27**, 109 (1994).
[7] P. Marte, R. Dum, R. Taïeb, P. Zoller, M. S. Shahriar, and M. Prentiss, Phys. Rev. A **49**, 4826 (1994).
[8] F. Mauri and E. Arimondo, Appl. Phys. B **54**, 420 (1992).
[9] M. S. Shahriar, P. R. Hemmer, M. G. Prentiss, A. Chu, D. P. Katz, and N. P. Bigelow, Opt. Commun. **103**, 453 (1992).
[10] M. Widmer *et al.* (unpublished).
[11] R. Kaiser, Ph.D. thesis, Université Paris 6, 1990 (unpublished).
[12] C. Cohen-Tannoudji, in *Frontiers in Laser Spectroscopy Vol. 1*, Proceedings of Les Houches Summer School of Theoretical Physics, Les Houches, 1990, edited by R. Balian, S. Haroche, and S. Liberman (North-Holland, Amsterdam, 1977).
[13] Y. Castin, J. Dalibard, and C. Cohen-Tannoudji, in *Light Induced Kinetic Effects on Atoms, Ions and Molecules*, Proceedings of the Workshop, Elba Island, 1990, edited by Luigi Moi *et al.* (ETS Editrice, Pisa, 1991).
[14] C. Cohen-Tannoudji, in *Laser Manipulation of Atoms and Ions*, Proceedings of the International School of Physics "Enrico Fermi," Course CXVIII, Varenna, 1991, edited by E. Arimondo, W. D. Phillips, and F. Strumia (North-Holland, Amsterdam, 1992).
[15] M. R. Doery, E. J. D. Vredenbregt, and T. Bergeman, Phys. Rev. A **51**, 4881 (1995).
[16] For σ^+-σ^- polarization gradient cooling on a $J_g = 1 \rightarrow J_e = 2$ transition, similar eigenvalues have been found by H. Wu and C. J. Foot, J. Phys. B **27**, L677 (1994).
[17] T. Bergeman, Phys. Rev. A **48**, R3425 (1993).
[18] A. Chu, M. Prentiss, D. P. Katz, M. S. Shahriar, P. R. Hemmer, P. Marte, and P. Zoller (private communication).
[19] M. Doery, M. Widmer, J. Bellanca, E. Vredenbregt, T. Bergeman, and H. Metcalf, Phys. Rev. Lett. **72**, 2546 (1994).
[20] T. Chuang, Ph.D. dissertation, State University of New York at Stony Brook, 1991 (unpublished).
[21] T. Chuang and H. J. Metcalf, Appl. Opt. **30**, 2495 (1992).
[22] T. P. Dinneen, C. D. Wallace, and P. L. Gould, Opt. Commun. **92**, 277 (1992).